

Article

Crystal Structure, Chemical Bonding and Magnetism Studies for Three Quinary Polar Intermetallic Compounds in the $(\text{Eu}_{1-x}\text{Ca}_x)_9\text{In}_8(\text{Ge}_{1-y}\text{Sn}_y)_8$ ($x = 0.66, y = 0.03$) and the $(\text{Eu}_{1-x}\text{Ca}_x)_3\text{In}(\text{Ge}_{3-y}\text{Sn}_{1+y})$ ($x = 0.66, 0.68; y = 0.13, 0.27$) Phases

Hyein Woo ¹, Eunyong Jang ¹, Jin Kim ², Yunho Lee ², Jongsik Kim ³ and Tae-Soo You ^{1,*}

¹ Department of Chemistry, Chungbuk National University, Cheongju, Chungbuk 362-763, Korea; E-Mails: hiwoo52@chungbuk.ac.kr (H.W.); s2jeyoung@chungbuk.ac.kr (E.J.)

² Department of Chemistry, Korea Advanced Institute of Science and Technology, Daejeon 305-701, Korea; E-Mails: kj0815@kaist.ac.kr (J.K.); yunholee@kaist.ac.kr (Y.L.)

³ Department of Chemistry, Dong-A University, Busan 604-714, Korea; E-Mail: jskimm@dau.ac.kr

* Author to whom correspondence should be addressed; E-Mail: tyou@chungbuk.ac.kr; Tel.: +82-43-261-2282; Fax: +82-43-267-2279.

Academic Editor: Habil. Mihai V. Putz

Received: 25 February 2015 / Accepted: 9 April 2015 / Published: 22 April 2015

Abstract: Three quinary polar intermetallic compounds in the $(\text{Eu}_{1-x}\text{Ca}_x)_9\text{In}_8(\text{Ge}_{1-y}\text{Sn}_y)_8$ ($x = 0.66, y = 0.03$) and the $(\text{Eu}_{1-x}\text{Ca}_x)_3\text{In}(\text{Ge}_{3-y}\text{Sn}_{1+y})$ ($x = 0.66, 0.68; y = 0.13, 0.27$) phases have been synthesized using the molten In-metal flux method, and the crystal structures are characterized by powder and single-crystal X-ray diffractions. Two orthorhombic structural types can be viewed as an assembly of polyanionic frameworks consisting of the $\text{In}(\text{Ge}/\text{Sn})_4$ tetrahedral chains, the bridging Ge_2 dimers, either the annulene-like “12-membered rings” for the $(\text{Eu}_{1-x}\text{Ca}_x)_9\text{In}_8(\text{Ge}_{1-y}\text{Sn}_y)_8$ series or the *cis-trans* Ge/Sn-chains for the $(\text{Eu}_{1-x}\text{Ca}_x)_3\text{In}(\text{Ge}_{3-y}\text{Sn}_{1+y})$ series, and several Eu/Ca-mixed cations. The most noticeable difference between two structural types is the amount and the location of the Sn-substitution for Ge: only a partial substitution (11%) occurs at the $\text{In}(\text{Ge}/\text{Sn})_4$ tetrahedron in the $(\text{Eu}_{1-x}\text{Ca}_x)_9\text{In}_8(\text{Ge}_{1-y}\text{Sn}_y)_8$ series, whereas both a complete and a partial substitution (up to 27%) are observed, respectively, at the *cis-trans* Ge/Sn-chain and at the $\text{In}(\text{Ge}/\text{Sn})_4$ tetrahedron in the $(\text{Eu}_{1-x}\text{Ca}_x)_3\text{In}(\text{Ge}_{3-y}\text{Sn}_{1+y})$ series. A series of tight-binding linear muffin-tin orbital calculations is conducted to understand overall electronic structures and chemical bonding among components. Magnetic susceptibility measurement indicates a ferromagnetic ordering of Eu atoms below 5 K for $\text{Eu}_{1.02(1)}\text{Ca}_{1.98}\text{InGe}_{2.87(1)}\text{Sn}_{1.13}$.

Keywords: polar intermetallics; electronic structure; chemical bonding; single-crystal X-ray diffraction; magnetism

1. Introduction

Polar intermetallic and Zintl phase compounds have been one of the most interesting research topics for solid-state chemists to investigate the co-relationship among composition-structure-property and to apply the obtained knowledge to various energy-related materials, such as thermoelectrics, magnetocalorics and magnetoresistance materials [1–6]. Among these compounds, the rare-earth metal containing compounds are worth exploring due to their intriguing chemical and physical characteristics derived by electrons in the $4f$ orbitals [7–11]. In particular, some polar intermetallics containing europium with the half-filled $4f$ orbitals are known to show anomalous magnetic properties [12–14].

Our group has continuously investigated rare-earth metal containing polar intermetallics as well as Zintl phase compounds and successfully synthesized several novel compounds as reported in recent articles [14–20]. As a part of our ongoing systematic investigations for the Eu-containing polar intermetallic compounds, we attempted to expand the variety of the recently reported $(\text{Eu}_{1-x}\text{Ca}_x)_9\text{In}_8\text{Ge}_8$ series by substituting elements and adjusting reaction conditions. The series of reaction attempts eventually revealed that the heavier Sn successfully replaced Ge in this series resulting in producing three title compounds: $\text{Eu}_{3.04(4)}\text{Ca}_{5.96}\text{In}_8\text{Ge}_{7.77(2)}\text{Sn}_{0.23}$, $\text{Eu}_{1.02(1)}\text{Ca}_{1.98}\text{InGe}_{2.87(1)}\text{Sn}_{1.13}$ and $\text{Eu}_{0.95(1)}\text{Ca}_{2.05}\text{InGe}_{2.73(1)}\text{Sn}_{1.27}$, which were the first three quinary derivatives from the $(\text{Eu}_{1-x}\text{Ca}_x)_9\text{In}_8\text{Ge}_8$ and the $(\text{Eu}_{1-x}\text{Ca}_x)_3\text{In}_2\text{Ge}_3$ series, respectively [12,14]. Interestingly, the amount and the location of the Sn-substitution for Ge differentiated two structural types: only a partial Sn substitution for Ge at the $\text{In}(\text{Ge}/\text{Sn})_4$ tetrahedron resulted in the $(\text{Eu}_{1-x}\text{Ca}_x)_9\text{In}_8(\text{Ge}_{1-y}\text{Sn}_y)_8$ series, whereas a partial and a complete Sn substitutions for Ge in the polyanionic framework produced the $(\text{Eu}_{1-x}\text{Ca}_x)_3\text{In}(\text{Ge}_{3-y}\text{Sn}_{1+y})$ series.

In this article, we report crystal structures of two title phases in terms of the amount and the location of the Sn-substitution and provide the rationale for these phenomena using the atomic size-factor perspective and comprehensive theoretical analyses. Tight-binding linear muffin-tin orbital (TB-LMTO) calculations [21–25] were conducted using two structural models with idealized compositions. Density of states (DOS) and crystal orbital Hamilton population (COHP) curves [26] were thoroughly studied to understand orbital contributions for particular energy regions and chemical bonding from interatomic interactions. Physical and chemical analyses including energy-dispersive X-ray spectroscopy (EDS), scanning electron microscope (SEM), differential scanning calorimeter (DSC), and magnetization were also performed.

2. Results and Discussion

2.1. Crystal Structure Descriptions

2.1.1. $(\text{Eu}_{1-x}\text{Ca}_x)_9\text{In}_8(\text{Ge}_{1-y}\text{Sn}_y)_8$ Phase

$\text{Eu}_{3.04(4)}\text{Ca}_{5.96}\text{In}_8\text{Ge}_{7.77(2)}\text{Sn}_{0.23}$ is the first quinary derivative of the recently reported $(\text{Eu}_{1-x}\text{Ca}_x)_9\text{In}_8\text{Ge}_8$ [14] series having a partial Sn-substitution for Ge. The title compound adopted its

parental $\text{Eu}_{2.94(2)}\text{Ca}_{6.06}\text{In}_8\text{Ge}_8$ -type structure and crystallized in the orthorhombic $Pm\bar{m}n$ space group ($Z = 2$, Pearson code $oP50$) with 14 crystallographically independent sites in the asymmetric unit (Table 1). The overall crystal structure is illustrated in Figure 1, and a SEM image of a needle-/bar-shaped single-crystal is also shown in Figure 2a.

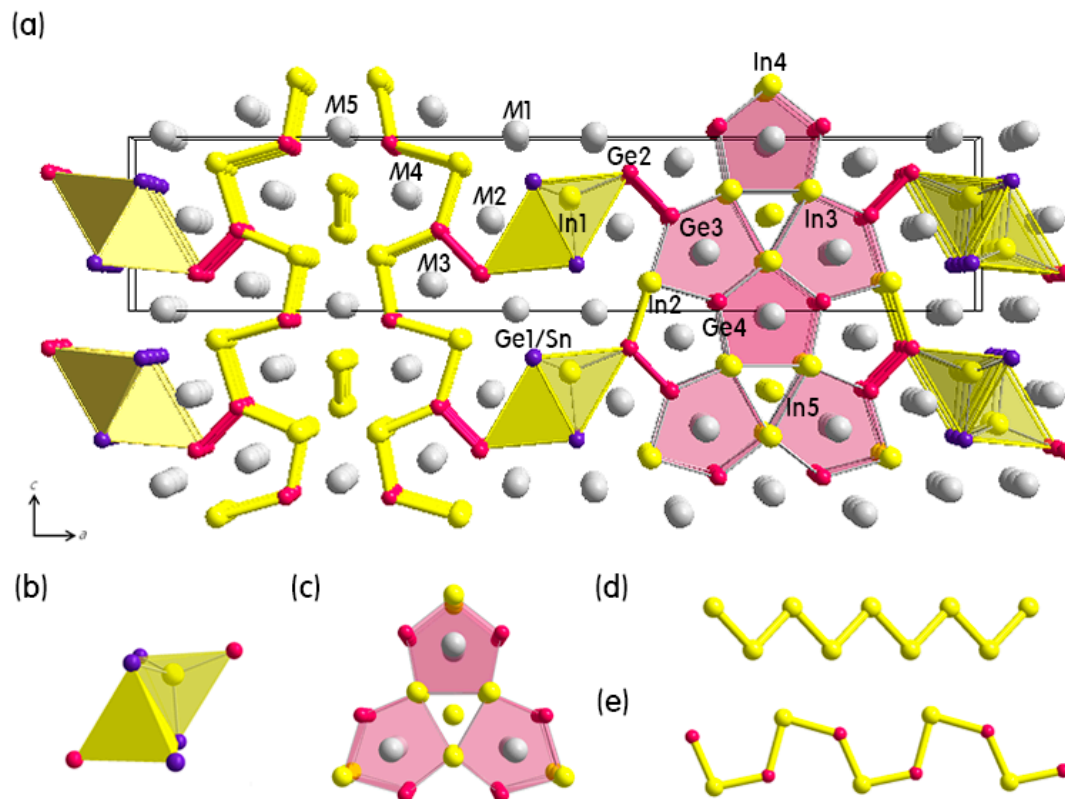


Figure 1. (a) Combined ball-and-stick and polyhedral representation for the crystal structure of the $(\text{Eu}_{1-x}\text{Ca}_x)_9\text{In}_8(\text{Ge}_{1-y}\text{Sn}_y)_8$ ($x = 0.66$, $y = 0.03$) series viewed down along the b -axis; (b) The edge-sharing $\text{In}(\text{Ge}/\text{Sn})_4$ tetrahedra; (c) The “12-membered rings”; (d) The 1D zig-zag In-chain; and (e) The 1D *cis-trans* Ge/In-chain are also illustrated. Unit cell is outlined in black. Color codes are as follows: M (Eu/Ca-mixed site), gray; Ge, magenta; Ge1/Sn-mixed site, purple; and In, yellow.

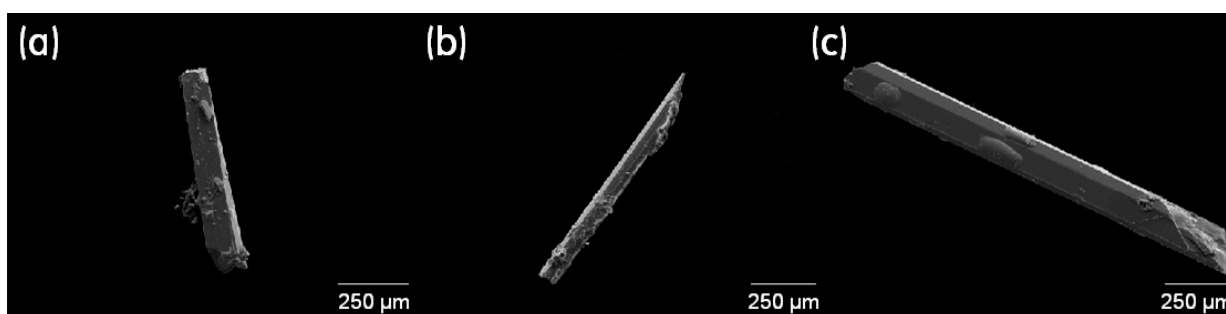


Figure 2. SEM images for bar-/needle-shaped single-crystals of (a) $\text{Eu}_{3.04(4)}\text{Ca}_{5.96}\text{In}_8\text{Ge}_{7.77(2)}\text{Sn}_{0.23}$; (b) $\text{Eu}_{1.02(1)}\text{Ca}_{1.98}\text{InGe}_{2.87(1)}\text{Sn}_{1.13}$; and (c) $\text{Eu}_{0.95(1)}\text{Ca}_{2.05}\text{InGe}_{2.73(1)}\text{Sn}_{1.27}$. Small amounts of In-flux metals remaining on the surface of single-crystals are also observed. Scale bar = 250 μm .

Table 1. Single-crystal crystallographic data and structure refinement results for $\text{Eu}_{3.04(4)}\text{Ca}_{5.96}\text{In}_8\text{Ge}_{7.77(2)}\text{Sn}_{0.23}$, $\text{Eu}_{1.02(1)}\text{Ca}_{1.98}\text{InGe}_{2.87(1)}\text{Sn}_{1.13}$ and $\text{Eu}_{0.95(1)}\text{Ca}_{2.05}\text{InGe}_{2.73(1)}\text{Sn}_{1.27}$.

Empirical Formula	$\text{Eu}_{3.04(4)}\text{Ca}_{5.96}\text{In}_8\text{Ge}_{7.77(2)}\text{Sn}_{0.23}$	$\text{Eu}_{1.02(1)}\text{Ca}_{1.98}\text{InGe}_{2.87(1)}\text{Sn}_{1.13}$	$\text{Eu}_{0.95(1)}\text{Ca}_{2.05}\text{InGe}_{2.73(1)}\text{Sn}_{1.27}$
fw, $\text{g}\cdot\text{mol}^{-1}$	2211.05	691.24	690.25
space group, Z	$Pm\bar{m}n$ (No. 59), 2		$Pnma$ (No. 62), 4
unit cell dimension, Å	$a = 36.963(2)$ $b = 4.5176(2)$ $c = 7.5155(3)$	$a = 7.4974(8)$ $b = 4.4847(4)$ $c = 23.819(3)$	$a = 7.5096(3)$ $b = 4.4959(2)$ $c = 23.8518(9)$
volume, Å ³	1254.97(9)	800.88(14)	805.29(6)
density (ρ_{calcd}), $\text{g}\cdot\text{cm}^{-3}$	5.851	5.733	5.693
absorption coefficient (μ), cm^{-1}	252.39	259.44	252.39
GOF on F^2	1.074	1.057	1.059
R^a [$I > 2\sigma(I)$]	$R_1 = 0.0348$ $wR_2 = 0.0595$	$R_1 = 0.0264$ $wR_2 = 0.0462$	$R_1 = 0.0256$ $wR_2 = 0.0400$
R [all data]	$R_1 = 0.0540$ $wR_2 = 0.0637$	$R_1 = 0.0399$ $wR_2 = 0.0541$	$R_1 = 0.0411$ $wR_2 = 0.0472$
largest diff. peak and hole, $\text{e}^{-}\cdot\text{Å}^{-3}$	2.423 and -2.527	1.180 and -1.821	1.859 and -1.585

^a $R_1 = \Sigma||F_o| - |F_c||/\Sigma|F_o|$; $wR_2 = [\Sigma[w(F_o^2 - F_c^2)]/\Sigma[w(F_o^2)^2]]^{1/2}$, where $w = 1/[\sigma^2 F_o^2 + (A \cdot P)^2 + B \cdot P]$, and $P = (F_o^2 + 2F_c^2)/3$; A and B are weight coefficients.

The overall crystal structure can be viewed as an assembly of the three-dimensional (3D) polyanionic framework consisting of three types of anions and five mixed-cationic sites embedded within the framework. Furthermore, the 3D framework can be understood as a combination of (1) the one-dimensional (1D) In(Ge/Sn)₄ tetrahedral chains extending along the *b*-axis direction and (2) the distorted annulene-like “12-membered rings”, which stacked on top of each other along the *b*-axis direction and eventually resulted in forming three edge-sharing pentagonal-prisms (See the right side of Figure 1). This anionic 12-membered ring can alternately be viewed as a combination of the 1D *zig-zag* In-chains (Figure 1d) and the 1D *cis-trans* Ge/In-chains (Figure 1e) propagating, respectively, along the *b*-axis and the *c*-axis as illustrated in the left side of Figure 1. According to this alternative perspective, the structure type of the (Eu_{1-x}Ca_x)₉In₈(Ge_{1-y}Sn_y)₈ phase can more easily be comparable to the other title phase, the (Eu_{1-x}Ca_x)₃In(Ge_{3-y}Sn_{1+y}) series, which will be discussed in a subsequent section. In addition, the In(Ge/Sn)₄ chains and the 12-membered rings are further connected via the Ge₂ dimers along the *a*-axis direction. Interestingly, the newly introduced Sn partially substituted for Ge (11%) only at the Ge1 site in the In(Ge/Sn)₄ tetrahedron among total nine anionic sites. The rest of Ge and In sites showed no sign of the Sn-substitution. The limited Sn-substitution at the Ge1 site is clearly distinctive from the Sn-substitution occurred in the (Eu_{1-x}Ca_x)₃In(Ge_{3-y}Sn_{1+y}) series. We will further discuss about the different Sn-substitutions in the subsequent section.

The overall crystal structure can be viewed as an assembly of the three-dimensional (3D) polyanionic framework consisting of three types of anions and five mixed-cationic sites embedded within the framework. Furthermore, the 3D framework can be understood as a combination of (1) the one-dimensional (1D) In(Ge/Sn)₄ tetrahedral chains extending along the *b*-axis direction and (2) the distorted annulene-like “12-membered rings”, which stacked on top of each other along the *b*-axis direction and eventually resulted in forming three edge-sharing pentagonal-prisms (See the right side of Figure 1). This anionic 12-membered ring can alternately be viewed as a combination of the 1D *zig-zag* In-chains (Figure 1d) and the 1D *cis-trans* Ge/In-chains (Figure 1e) propagating, respectively, along the *b*-axis and the *c*-axis as illustrated in the left side of Figure 1. According to this alternative perspective, the structure type of the (Eu_{1-x}Ca_x)₉In₈(Ge_{1-y}Sn_y)₈ phase can more easily be comparable to the other title phase, the (Eu_{1-x}Ca_x)₃In(Ge_{3-y}Sn_{1+y}) series, which will be discussed in a subsequent section. In addition, the In(Ge/Sn)₄ chains and the 12-membered rings are further connected via the Ge₂ dimers along the *a*-axis direction. Interestingly, the newly introduced Sn partially substituted for Ge (11%) only at the Ge1 site in the In(Ge/Sn)₄ tetrahedron among total nine anionic sites. The rest of Ge and In sites showed no sign of the Sn-substitution. The limited Sn-substitution at the Ge1 site is clearly distinctive from the Sn-substitution occurred in the (Eu_{1-x}Ca_x)₃In(Ge_{3-y}Sn_{1+y}) series. We will further discuss about the different Sn-substitutions in the subsequent section.

The similar types of edge-sharing In(Ge/Sn)₄ tetrahedral chains have been frequently reported in several recent articles [12,14,20]. In particular, the observed In1-Ge/Sn bond distances in Eu_{3.04(4)}Ca_{5.96}In₈Ge_{7.77(2)}Sn_{0.23} are 2.816 and 2.896 Å, which are well comparable to the values reported in some compounds: 2.769–2.909 Å in the M₉In₈Ge₈ (*M* = Eu/Ca-, Sr/Ca-mixed sites) [14], 2.802–2.887 Å in the (Eu_{1-x}Ca_x)₄In₃Ge₄ (0.35 ≤ *x* ≤ 0.70) [12], 2.790–2.869 Å in the (Eu_{1-x}Ca_x)₃In₂Ge₃ (0.78 ≤ *x* ≤ 0.90) [12], 2.716–2.822 Å in the (Sr_{1-x}Ca_x)₃In₂Ge₄ (*x* = 0.39, 0.49) series [20], and 2.672–2.877 Å in Sr_{1.50}Ca_{3.50}In₃Ge₆ [20]. It is noteworthy to mention that the size of a unit cell (Table 1) involving the In1-Ge/Sn distances in the title compound is not much expanded as compared to those in the parental

(Eu_{1-x}Ca_x)₉In₈Ge₈ series [14] as well as above mentioned examples in spite of the large size difference between Sn and Ge ($r_{\text{Sn}} = 1.40 \text{ \AA}$, $r_{\text{Ge}} = 1.22 \text{ \AA}$) [27]. The rationale for this observation can surely be provided by a relatively small amount of the Sn substitution only at the Ge1 site, which is not the case of the other title phase, the (Eu_{1-x}Ca_x)₃In(Ge_{3-y}Sn_{1+y}) series. The Ge-Ge bond distance of the Ge₂ dimer is 2.554 Å. This value is also well comparable to those observed in above examples including 2.551–2.567 Å in the M₉In₈Ge₈ (M = Eu/Ca- or Sr/Ca-mixed sites) [14], 2.54 Å in the (Eu_{1-x}Ca_x)₄In₃Ge₄ (0.35 ≤ x ≤ 0.70) [12], 2.527–2.533 Å in the M₃In₂Ge₃ (M = Eu/Ca-mixed sites) [12], 2.538–2.622 Å in the (Sr_{1-x}Ca_x)₃In₂Ge₄ (x = 0.39, 0.49) series [20], and 2.528–2.550 Å in Sr_{1.50}Ca_{3.50}In₃Ge₆ [20].

As briefly mentioned earlier, there exist five asymmetric Eu/Ca mixed-sites, which are surrounded by Ge and In. In particular, the M1 site having ca. 30% of Eu occupation has a total coordination number of 9 and shows the distorted square-pyramidal coordination environment. The rest of four cationic sites having a total coordination number of 10 are surrounded by the pentagonal-prismatic environments: the M2 and the M3 sites are coordinated by six Ge (or Ge/Sn) and four In atoms, whereas the M4 and the M5 sites are coordinated by six In and four Ge atoms (Figure 1 and Table 2).

Table 2. Atomic coordinates, occupation factors and equivalent isotropic displacement parameters (U_{eq}^a) from single-crystal structure refinements for Eu_{3.04(4)}Ca_{5.96}In₈Ge_{7.77(2)}Sn_{0.23}, Eu_{1.02(1)}Ca_{1.98}InGe_{2.87(1)}Sn_{1.13} and Eu_{0.95(1)}Ca_{2.05}InGe_{2.73(1)}Sn_{1.27}.

Atom	Wyckoff Site	Occupation Factor	x	y	z	U_{eq}^a (Å ²)
Eu _{3.04(4)} Ca _{5.96} In ₈ Ge _{7.77(2)} Sn _{0.23}						
M1 ^b	4f	0.298(4)/0.702	0.0456 (1)	1/4	0.0079(2)	0.0066(5)
M2 ^b	4f	0.506(4)/0.494	0.0755(1)	1/4	0.5209(1)	0.0053(3)
M3 ^b	4f	0.271(4)/0.729	0.1443(1)	1/4	0.1498(2)	0.0055(5)
M4 ^b	4f	0.284(4)/0.716	0.1740(1)	1/4	0.6668(2)	0.0060(5)
M5 ^b	2a	0.325(6)/0.675	1/4	1/4	0.0310(3)	0.0068(6)
In1	4f	1	0.5172(1)	1/4	0.6502(1)	0.0052(2)
In2	4f	1	0.6110(1)	1/4	0.1632(1)	0.0077(2)
In3	4f	1	0.7039(1)	1/4	0.6868(1)	0.0055(2)
In4	2b	1	3/4	1/4	0.2854(2)	0.0068(3)
In5	2a	1	1/4	1/4	0.4544(2)	0.0074(3)
Ge1/Sn	4f	0.887(12)/0.113	0.5251(1)	1/4	0.2668(2)	0.0072(4)
Ge2	4f	1	0.5867(1)	1/4	0.7882(2)	0.0050(3)
Ge3	4f	1	0.6344(1)	1/4	0.5427(2)	0.0050(3)
Ge4	4f	1	0.6898(1)	1/4	0.0519(2)	0.0043(3)
Eu _{1.02(1)} Ca _{1.98} InGe _{2.87(1)} Sn _{1.13}						
M1 ^b	4c	0.302(3)/0.698	0.0096(1)	1/4	0.0735(1)	0.0070(3)
M2 ^b	4c	0.483(3)/0.517	0.0273(1)	1/4	0.3814(1)	0.0066(2)
M3 ^b	4c	0.232(3)/0.768	0.1640(1)	1/4	0.2267(1)	0.0080(3)
In1	4c	1	0.1497(1)	1/4	0.5283(1)	0.0074(1)
Sn1	4c	1	0.1623(1)	1/4	0.8244(1)	0.0096(1)
Ge1	4c	1	0.0391(1)	1/4	0.7108(1)	0.0060(2)
Ge2	4c	1	0.2833(1)	1/4	0.6371(1)	0.0063(2)
Ge3/Sn2	4c	0.871(7)/0.129	0.7643(1)	1/4	0.5375(1)	0.0065(2)

Table 2. Cont.

Atom	Wyckoff Site	Occupation Factor	x	y	z	U_{eq}^a (Å ²)
		Eu _{0.95(1)} Ca _{2.05} InGe _{2.73(1)} Sn _{1.27}				
M1 ^b	4c	0.274(2)/0.726	0.0106(1)	1/4	0.0740(1)	0.0077(2)
M2 ^b	4c	0.453(2)/0.547	0.0264(1)	1/4	0.3811(1)	0.0064(2)
M3 ^b	4c	0.220(2)/0.780	0.1642(1)	1/4	0.2269(1)	0.0070(2)
In1	4c	1	0.1505(1)	1/4	0.5287(1)	0.0077(1)
Sn1	4c	1	0.1624(1)	1/4	0.8243(1)	0.0088(1)
Ge1	4c	1	0.0395(1)	1/4	0.7108(1)	0.0062(1)
Ge2	4c	1	0.2837(1)	1/4	0.6374(1)	0.0064(1)
Ge3/Sn2	4c	0.734(7)/0.266	0.7635(1)	1/4	0.5377(1)	0.0067(2)

^a U_{eq} is defined as one third of the trace of the orthogonalized U_{ij} tensor; ^b M is refined as statistical mixture of Eu and Ca.

2.1.2. (Eu_{1-x}Ca_x)₃In(Ge_{3-y}Sn_{1+y}) Phase

Two quinary derivatives of Eu_{1.02(1)}Ca_{1.98}InGe_{2.87(1)}Sn_{1.1.03} and Eu_{0.95(1)}Ca_{2.05}InGe_{2.73(1)}Sn_{1.27} in the (Eu_{1-x}Ca_x)₃In(Ge_{3-y}Sn_{1+y}) phase have been serendipitously produced when the reaction condition satisfied two following criteria: (1) the loaded Sn content increased up to equal to or slightly higher than the loaded Ge content and (2) the loaded ratio between Eu/Ca- and Ge/Sn-mixture was 1:1. Interestingly, according to a recent article about the (Eu_{1-x}Ca_x)₄In₃Ge₄ and the (Eu_{1-x}Ca_x)₃In₂Ge₃ series [12], either one of two phases could selectively be produced by controlling the loaded ratio between Eu and Ca. For instance, the (Eu_{1-x}Ca_x)₄In₃Ge₄ phase was produced when the ratio varied between *ca.* 2:1 and 1:2, whereas the (Eu_{1-x}Ca_x)₃In₂Ge₃ phase was obtained only when the loaded Ca content was at least three times larger than Eu, such as Eu:Ca = 1:3 or 1:9. However, in this study, we revealed that two quinary derivatives from the (Eu_{1-x}Ca_x)₃In(Ge_{3-y}Sn_{1+y}) phase could possibly be obtained even when the loaded Ca contents were much smaller than those claimed in the earlier report, such as Eu:Ca = 1:1.94 and 1:2.16. In addition, the overall atomic % of Eu in title compounds was different from those in the parental (Eu_{1-x}Ca_x)₃In₂Ge₃ phase, which could not exceed 20% under any attempted reaction conditions. The rationale behind the limited Eu content was attributed to the fact that packing two different size cations in an ordered manner provided very little energy profit [12]. However, in the title phase, it increased up to 34 atomic % and could be explained by the atomic size-factor: the larger-size Sn atoms substituted the smaller-size Ge atoms not only at the vertex of the In(Ge/Sn)₄ tetrahedron, but also on the 1D *cis-trans* chain. As a result, an overall size of the unit cell including the 3D anionic framework expanded large enough to accommodate extra amounts of Eu.

Two title compounds in the (Eu_{1-x}Ca_x)₃In(Ge_{3-y}Sn_{1+y}) phase adopted the orthorhombic space group *Pnma* ($Z = 4$, Pearson code *oP32*) and contained eight crystallographically independent atomic sites in the asymmetric unit as provided in Tables 1 and 2. The overall crystal structure can be viewed as an assembly of three structural moieties: (1) the 1D edge-sharing In(Ge/Sn)₄ tetrahedral chains propagating along the *b*-axis direction; (2) the infinite *cis-trans* Ge/Sn-chains extending along the *a*-axis direction and (3) the Ge₂ dimers bridging these two structural moieties as illustrated in Figure 3. SEM images of two needle-/bar-shaped single-crystals are also displayed in Figure 2b,c. The In(Ge/Sn)₄ tetrahedral chain resembles the chain observed in Eu_{3.04(4)}Ca_{5.96}In₈Ge_{7.77(2)}Sn_{0.23} including a partial Sn substitution

for Ge, and the In-Ge/Sn bond distances in the tetrahedron (2.779 and 2.914 Å) are well comparable to those in $\text{Eu}_{3.04(4)}\text{Ca}_{5.96}\text{In}_8\text{Ge}_{7.77(2)}\text{Sn}_{0.23}$ as well as in some compounds discussed earlier. In particular, the infinite *cis-trans* Ge/Sn-chains, in which Ge and Sn atoms were alternately arranged in the *cis*- and *trans*-conformation, showed the relatively longer Ge-Sn bond distances (2.859 and 2.861 Å) than the sum of covalent radii of Ge and Sn (2.62 Å = 1.22 Å(r_{Ge}) + 1.40 Å(r_{Sn})) [27]. Lastly, the Ge–Ge distances of the Ge_2 dimer in two title compounds were nearly identical, 2.534 and 2.536 Å, and these values were also comparable to those in $\text{Eu}_{3.04(4)}\text{Ca}_{5.96}\text{In}_8\text{Ge}_{7.77(2)}\text{Sn}_{0.23}$ and in the parental $(\text{Eu}_{1-x}\text{Ca}_x)_3\text{In}_2\text{Ge}_3$ series [12].

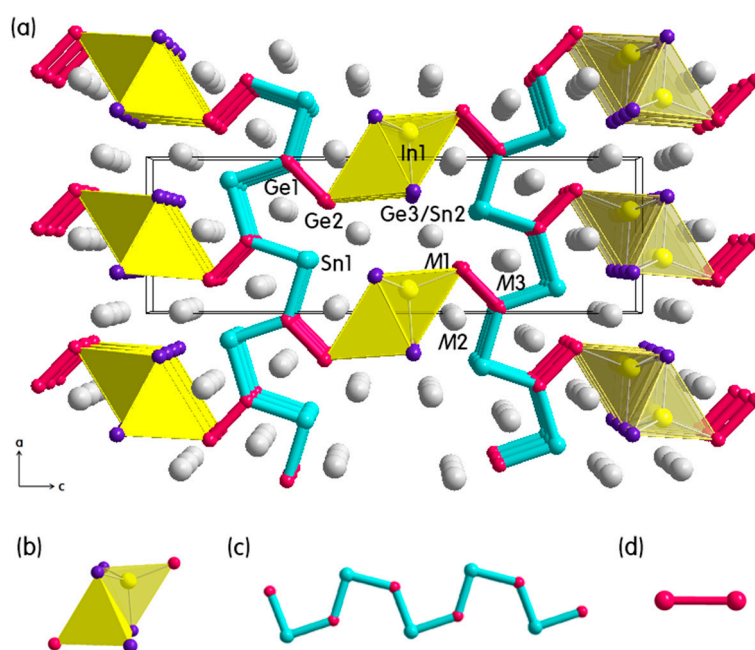


Figure 3. (a) Combined ball-and-stick and polyhedral representation for the crystal structure of the $(\text{Eu}_{1-x}\text{Ca}_x)_3\text{In}(\text{Ge}_{3-y}\text{Sn}_{1+y})$ ($x = 0.66, 0.68; y = 0.13, 0.27$) phase viewed down along the *b*-axis; (b) The edge-sharing $\text{In}(\text{Ge}/\text{Sn})_4$ tetrahedra; (c) The 1D *cis-trans* Ge/Sn-chains; and (d) The Ge_2 dimers are highlighted in yellow, light-blue, and magenta, respectively. Unit cell is outlined in black, and color codes are as follows: *M* (Eu/Ca-mixed site), gray; Ge, magenta; Ge/Sn mixed-site, purple; In, yellow; and Sn, light blue.

As briefly mentioned earlier, the crystal structure of the $(\text{Eu}_{1-x}\text{Ca}_x)_3\text{In}(\text{Ge}_{3-y}\text{Sn}_{1+y})$ phase can be compared with that of the $(\text{Eu}_{1-x}\text{Ca}_x)_9\text{In}_8(\text{Ge}_{1-y}\text{Sn}_y)_8$ phase. Firstly, both phases contain the common structural moieties including the edge-sharing $\text{In}(\text{Ge}/\text{Sn})_4$ tetrahedra and the *cis-trans* Ge/In- or Ge/Sn-chains. However, the $(\text{Eu}_{1-x}\text{Ca}_x)_9\text{In}_8(\text{Ge}_{1-y}\text{Sn}_y)_8$ phase exclusively includes the additional 1D *zig-zag* In-chains propagating along the *b*-axis and perpendicular to the *cis-trans* In/Ge-chains. In addition, the crystal structure contains two crystallographic mirror planes, respectively, along the $(1/4\ 0\ 0)$ and $(3/4\ 0\ 0)$ planes containing those *zig-zag* In-chains. Furthermore, the $(\text{Eu}_{1-x}\text{Ca}_x)_3\text{In}(\text{Ge}_{3-y}\text{Sn}_{1+y})$ -type structure is very closely related to the previously reported the $(\text{Eu}_{1-x}\text{Ca}_x)_4\text{In}_3\text{Ge}_4$ phase [12], in which the isotypic InTt_4 ($Tt = \text{Tetrels}$) tetrahedra with the Ge_2 dimers (previously-called “dumbbells”) were

connected directly to each other along the *a*-axis and via In atoms along the *c*-axis. Therefore, all these three phases can also be regarded as an intergrowth series with slightly different structural moieties.

It is noteworthy to mention that the most noticeable difference between the $(\text{Eu}_{1-x}\text{Ca}_x)_9\text{In}_8(\text{Ge}_{1-y}\text{Sn}_y)_8$ and the $(\text{Eu}_{1-x}\text{Ca}_x)_3\text{In}(\text{Ge}_{3-y}\text{Sn}_{1+y})$ phases was the amount and the location of Sn-substitution: in the $(\text{Eu}_{1-x}\text{Ca}_x)_9\text{In}_8(\text{Ge}_{1-y}\text{Sn}_y)_8$ phase, the 11% of Sn-substitution was successfully demonstrated only at one vertex of $\text{In}(\text{Ge}/\text{Sn})_4$ tetrahedron; whereas, in the $(\text{Eu}_{1-x}\text{Ca}_x)_3\text{In}(\text{Ge}_{3-y}\text{Sn}_{1+y})$ phase, not only the partial Sn-substitution (*ca.* 13% or 27%) occurred at one vertex of the tetrahedron, but also the complete substitution happened at one Ge site on the *cis-trans* chain. Therefore, if the Zintl-Klemm concept is applied to this phase, the chemical formula can be re-written as $[(\text{Eu}^{2+})_{1-x}(\text{Ca}^{2+})_x]_3[(\text{In}^-)(\text{Ge}^-)_{3-y}(\text{Sn}^-)_{1+y}] \cdot (1e^-)$, where a slightly charge-unbalanced formula should be expected. In addition, this chemical formula can explain the metallic property of the $(\text{Eu}_{1-x}\text{Ca}_x)_3\text{In}(\text{Ge}_{3-y}\text{Sn}_{1+y})$ phase represented by the following DOS curves shown in Figure 4b.

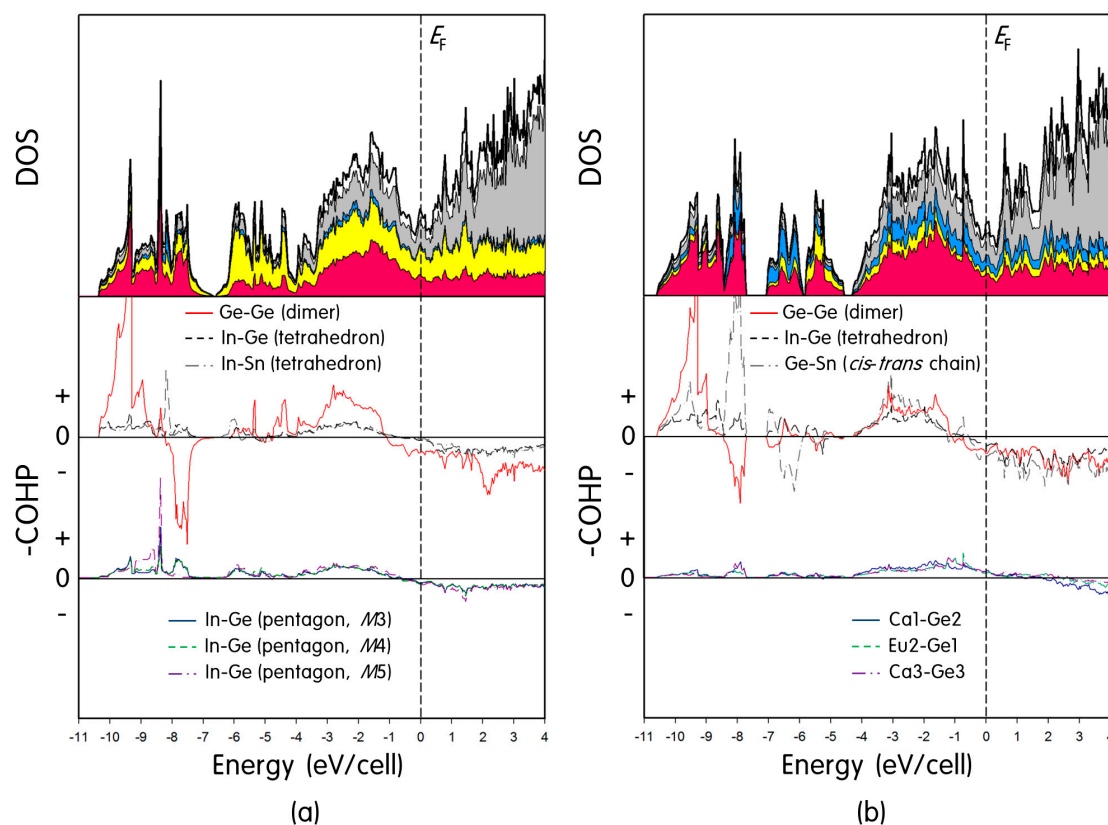


Figure 4. Density of states (DOS) and crystal orbital Hamilton population (COHP) curves for (a) “ $\text{Eu}_3\text{Ca}_6\text{In}_8\text{Ge}_7\text{Sn}$ ” and (b) “ $\text{EuCa}_2\text{InGe}_3\text{Sn}$ ”. Total and partial DOS curves are represented, respectively, by a solid-line and shaded areas with different colors as follows: Eu, white; Ca, gray; Sn, light blue; In, yellow; and Ge, magenta area. E_F (vertical line) is shown as a reference at 0 eV. Individual COHP curve is displayed: Ge-Ge forming the Ge_2 dimer, In-Ge and In-Sn forming the $\text{In}(\text{Ge}/\text{Sn})_4$ tetrahedron, In-Ge forming different pentagons, Ge-Sn forming the *cis-trans* Ge/Sn-chain, and three cation-anion interactions. In the $-\text{COHP}$ curves, the positive (“+”) values represent bonding interactions, whereas the negative (“-”) values represent antibonding interactions, respectively. The $-\text{COHP}$ curves for each model are plotted in the same scale, respectively.

2.2. Electronic Structure Calculations

A series of theoretical investigations have been systematically conducted using TB-LMTO method [24] to understand overall electronic structures of two title phases and chemical bonding among components [28–30]. Given the practical reason, a mixed-occupation of two atoms at one atomic site cannot be applied to computational calculations. Therefore, two structural models with idealized compositions of “Eu₃Ca₆In_{8–7}Sn” and “EuCa₂InGe₃Sn”, respectively, representing the (Eu_{1–x}Ca_x)₉In₈(Ge_{1–y}Sn_y)₈ and the (Eu_{1–x}Ca_x)₃In(Ge_{3–y}Sn_{1+y}) phases were designed and exploited for our theoretical studies.

2.2.1. Eu₃Ca₆In₈Ge₇Sn

To build a model with an idealized composition of Eu₃Ca₆In₈Ge₇Sn, firstly the experimentally obtained space group *Pmmn* was replaced by *Pmm2* to divide one Ge1/Sn mixed-site (*Wyckoff 4f*) into two individual sites (*Wyckoff 2e* and *2f*), and then Ge and Sn atoms were allocated to each site accordingly. In addition, two mixed-cationic sites having the larger Eu contents than other sites (*M2* and *M5*) were solely assigned for Eu, whereas the rest of three mixed-cationic sites (*M1*, *M3* and *M4*) were assigned for Ca. TB-LMTO calculations were executed using this structural model, and the resultant DOS and COHP curves are displayed in Figure 4a. Total and partial DOS curves show an overall valence orbital mixing of five components throughout the entire energy window. The local DOS minimum (so-called pseudogap) is observed at the Fermi level (E_F) implying a semi-metallic property of this phase, just like its parental (Eu_{1–x}Ca_x)₉In₈Ge₈ phase.

Total DOS curve can roughly be divided into three sectors below E_F . The sector between –10.5 and –7 eV displays several large peaks, which represent Ge σ_s bonding- and σ_s^* antibonding-states originated from the bridging Ge₂ dimer. The sector between –7 and –4 eV includes strong contributions descended from In 5*p* and Ge 4*p* states consisting of the 12-membered ring. Lastly, the sector from –4 to 0 eV shows significant contributions from In 5*p* and Ge 4*p* states with small additions from Sn 4*p* states, respectively, consisting of the In(Ge/Sn)₄ tetrahedron and the Ge₂ dimer. In particular, the noticeably large contributions from Eu and Ca are also observed in this sector implying that some degrees of bonding interactions between cations and anions should exist. This is one of the typical features of polar intermetallic compounds, which is caused by an incomplete electron transfer from cations to anions. Six COHP curves are also displayed in the middle and the bottom of Figure 4a. The Ge-Ge COHP curve from the Ge₂ dimer shows a strong anti-bonding character at E_F , whereas the In-Ge and the In-Sn COHP curves from the In(Ge/Sn)₄ tetrahedron are optimized at E_F . Three In-Ge COHPs representing various interactions on the 12-membered ring indicate relatively weak, but nearly optimized, interactions at E_F .

2.2.2. EuCa₂InGe₃Sn

For the structural model representing the (Eu_{1–x}Ca_x)₃In(Ge_{3–y}Sn_{1+y}) phase, the orthorhombic space group *Pnma* was exploited as obtained from the SXRD refinement. However, the *M2* site showing the largest Eu content among three mixed-cationic sites was solely assigned for Eu, and two other cationic sites were assigned for Ca. In addition, the mixed-site occupied by Ge₃ and Sn₂ was fully allocated by Ge to fulfill the idealized composition. It is noteworthy to mention that the Eu partial occupations over

three mixed-cationic sites in the title phase resembled the partial occupation trend observed in the parental $(\text{Eu}_{1-x}\text{Ca}_x)_3\text{In}_2\text{Ge}_3$ phase, where the largest Eu content was found at the $M2$ site, then the next largest one at the $M1$ site. The $M3$ site showed the smallest amount of Eu. The rationales for this site-preference of Eu were thoroughly investigated using both the coloring-problem and the QVAL value criteria in the earlier article [14].

A series of calculations was performed using $\text{EuCa}_2\text{InGe}_3\text{Sn}$, and DOS and COHP curves are illustrated in Figure 4b. The overall DOS curves and the location of E_F are similar to those obtained from $\text{Eu}_3\text{Ca}_6\text{In}_8\text{Ge}_7\text{Sn}$ as compared in Figure 4. In addition, the total DOS curve below E_F can roughly be divided into three sectors as well. However, the specific orbital contributions to these sectors were slightly different from those in $\text{Eu}_3\text{Ca}_6\text{In}_8\text{Ge}_7\text{Sn}$. In particular, the sector between -10.5 and -7.5 eV is mostly contributed by Ge $4s$ and Sn $5s$ orbitals originated, respectively, from bonding- and antibonding-states of the Ge_2 dimers, and bonding-states of the $1D$ *cis-trans* Ge/Sn chains. The sector between -7 and -4.5 eV has contributions from Ge $4s$, Sn $5s$ and In $5s$ orbitals from antibonding-states of the infinite *cis-trans* Ge/Sn-chain and bonding-/antibonding-states of the $\text{In}(\text{Ge}/\text{Sn})_4$ tetrahedron, respectively. Lastly, the sector between -4 and 0 eV displays a strong orbital mixing of Ge $4p$, In $5p$ and Sn $5p$ states with some contributions from two cations. Two COHP curves of the Ge-Ge and the Ge-Sn bonding, respectively, from the Ge_2 dimer and the *cis-trans* Ge/Sn chain display small antibonding characters at E_F , whereas the In-Ge COHP from the $\text{In}(\text{Ge}/\text{Sn})_4$ tetrahedron is nearly optimized at E_F . Three COHP curves representing interatomic interactions between cations and anions (Ca1-Ge2, Eu2-Ge1, and Ca3-Ge3) show relatively weak and small bonding characters (bottom of Figure 4b). These favorable bonding interactions can compensate several unfavorable antibonding characters descended from the Ge-Ge and the Ge-Sn bonding and eventually stabilize the overall crystal structure in the given chemical composition.

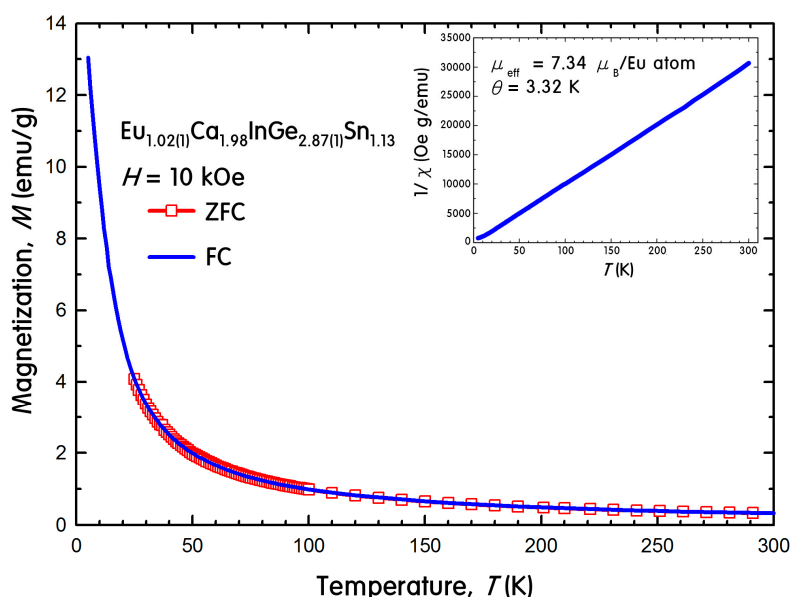


Figure 5. Magnetization of $\text{Eu}_{1.02(1)}\text{Ca}_{1.98}\text{InGe}_{2.87(1)}\text{Sn}_{1.13}$ as a function of temperature measured in dc magnetic field of 10 kOe under both ZFC and FC conditions. Inset shows the linear fit of temperature-dependent inverse magnetic susceptibility measured in 10 kOe under the FC condition.

2.3. Physical Property Measurements

The temperature-dependent dc magnetization was measured on a polycrystalline sample of $\text{Eu}_{1.02(1)}\text{Ca}_{1.98}\text{InGe}_{2.87(1)}\text{Sn}_{1.13}$ to study the magnetic interactions between Eu atoms. Since the magnetization study for the parental $(\text{Eu}_{1-x}\text{Ca}_x)_3\text{In}_2\text{Ge}_3$ phase was unsuccessful due to the presence of a secondary phase in products, the current magnetic property for its quinary derivative is the first report for its kind. Figure 5 illustrates the magnetization as a function of temperature between 5 and 300 K under zero-field cooled (ZFC) and field cooled (FC) conditions using the dc magnetic field of 10 kOe. The inverse susceptibility is also shown as a function of temperature in inset.

$\text{Eu}_{1.02(1)}\text{Ca}_{1.98}\text{InGe}_{2.87(1)}\text{Sn}_{1.13}$ followed the Curie-Weiss law with the corresponding paramagnetic behavior, and there was no indication of magnetic ordering down to 5 K. The effective magnetic moment of $7.34 \mu_B$ per Eu^{2+} ion was calculated from a linear fit of the inverse magnetic susceptibility *versus* temperature, and this value was relatively lower than the theoretically expected effective moment of $7.94 \mu_B$ for a free Eu^{2+} ion. This kind of discrepancy between the experimental and the theoretical values was previously reported in our recent article about $\text{Eu}_{3.13(2)}\text{Ca}_{5.87}\text{In}_8\text{Ge}_8$, which was also synthesized by the molten In-metal flux method. The reason for this discrepancy was attributed to small amounts of remaining In metals even after the centrifugation conducted at the last stage of the flux reaction. The inclusion of In metals in our product was verified by powder X-ray diffraction (PXRD) (Figure 6), DSC (Figure 7) and SEM images analyses. The extrapolation of the linear fitting for the magnetic susceptibility curve in the paramagnetic region resulted in $\theta_P = +3.32$ K, which indicated a weak and relatively low temperature ferromagnetic (FM) ordering of Eu atoms.

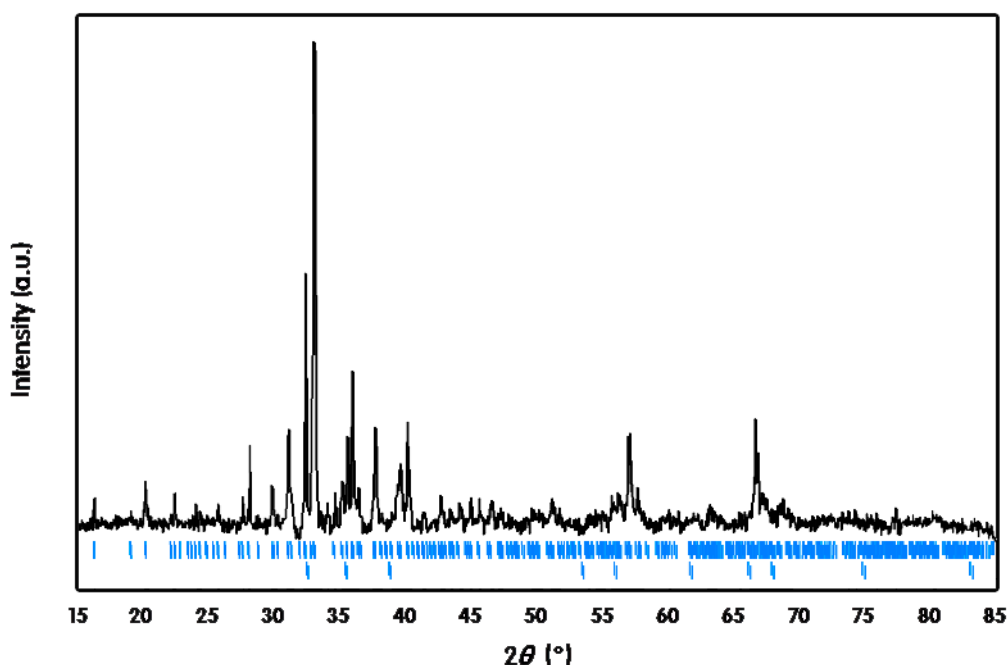


Figure 6. Powder X-ray diffraction (PXRD) pattern of $\text{Eu}_{1.02(1)}\text{Ca}_{1.98}\text{InGe}_{2.87(1)}\text{Sn}_{1.13}$. The upper and lower ticks shown in blue indicate the calculated reflection positions of $\text{Eu}_{1.02(1)}\text{Ca}_{1.98}\text{InGe}_{2.87(1)}\text{Sn}_{1.13}$ and elemental In, respectively.

Figure 7 displays a DSC curve plotting the heat flow as a function of temperature change between 300 and 770 K. No exothermic or endothermic peak was observed except a peak at 420 K originated from In metal. This implies that there exists no impurity phase in a product and no possibility of structural transformation or decomposition of the product in the measured temperature range.

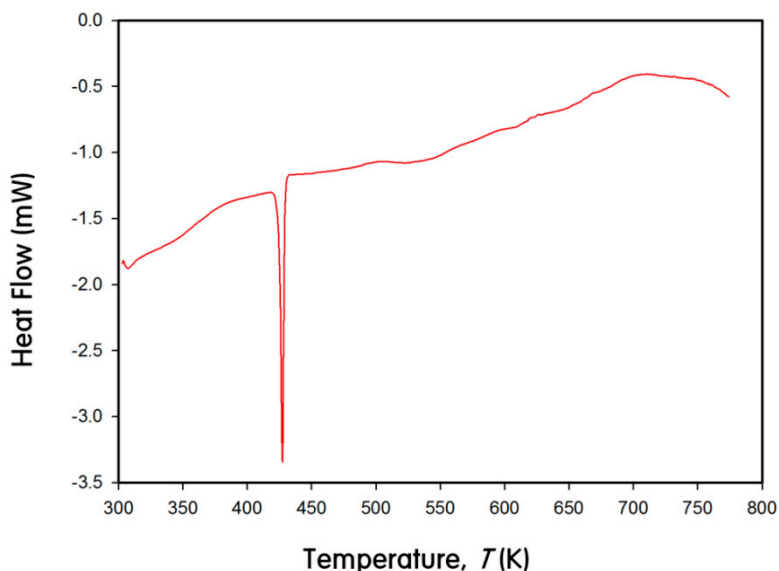


Figure 7. Differential scanning calorimeter (DSC) curve for $\text{Eu}_{1.02(1)}\text{Ca}_{1.98}\text{InGe}_{2.87(1)}\text{Sn}_{1.13}$ between 300 and 770 K.

3. Experimental Section

3.1. Synthesis

All manipulations during the synthesis were carried out in an argon-filled glove-box with O_2 and H_2O contents of <0.1 ppm or under vacuum. The starting materials were used as purchased from Alfa, and the list of materials is as follows: Eu—ingot, 99.9%; Ca—shot, 99.5%; In—tear drop, 99.99%; Ge—pieces, 99.999%; and Sn—shot, 99.99%. Tanned surface of the Eu ingot was scrapped off using a scalpel before loaded in a reaction container. The molten In-metal flux reaction, in which excess amounts of In metals were used as a reactive flux, was carried out in an alumina crucible (*ca.* 2 cm^3), and the loaded elemental ratios were $\text{Eu}:\text{Ca}:\text{Ge}:\text{Sn}:\text{In} = 0.9:1.1:(1-x):x:8$ ($x = 0.1\text{--}0.3$) and $0.9:1.1:(2-x):x:8$ ($x = 1.0\text{--}1.2$), respectively, for derivatives of the $(\text{Eu}_{1-x}\text{Ca}_x)_9\text{In}_8(\text{Ge}_{1-y}\text{Sn}_y)_8$ and the $(\text{Eu}_{1-x}\text{Ca}_x)_3\text{In}(\text{Ge}_{3-y}\text{Sn}_{1+y})$ phases. After each elemental mixture was loaded in a reaction container, it was subsequently enclosed in a fused-silica ampoule by flame-sealing under vacuum. Then, the fused-silica ampoule was heated up to $960 \text{ }^\circ\text{C}$ at the rate of $200 \text{ }^\circ\text{C/h}$ by a box-type furnace, held there for 20 h, then cooled down to $500 \text{ }^\circ\text{C}$ at the rate of $5 \text{ }^\circ\text{C/h}$. The extra amounts of molten In metals were removed by the instantaneous centrifugation at $500 \text{ }^\circ\text{C}$. Large amounts of well-grown bundles of bar-/needle-shaped single-crystals with a silver luster were obtained from all three products. $\text{Eu}_{3.04(4)}\text{Ca}_{5.96}\text{In}_8\text{Ge}_{7.77(2)}\text{Sn}_{0.23}$ was air-/moisture-sensitive and started to decompose after one day, whereas two compounds in the $(\text{Eu}_{1-x}\text{Ca}_x)_3\text{In}(\text{Ge}_{3-y}\text{Sn}_{1+y})$ phase remained intact at least for one week.

3.2. Crystal Structure Determinations

Crystal structures of three title compounds have been characterized by both powder and single-crystal X-ray diffractions (SXR). Powder X-ray diffraction (PXRD) patterns were obtained using Bruker D8 diffractometer (monochromatic Cu $K\alpha_1$ radiation, $\lambda = 1.54059 \text{ \AA}$) with a step size of 0.05° in the range of $15^\circ \leq 2\theta \leq 85^\circ$ and a total exposure time of 1 h. Primarily, a phase purity of each product was briefly checked, and lattice parameters of each unit cell were obtained using program *Rietica* [31]. Several peaks originated from remaining In metals were also indexed. SXR data were collected using Bruker SMART APEX2 CCD-based diffractometer (Bruker, Billerica, MA, USA) equipped with Mo $K\alpha_1$ radiation ($\lambda = 0.71073 \text{ \AA}$) at room temperature. Firstly, several silvery lustrous bar-/needle-shaped single-crystals were isolated and selected from bundles or aggregates of each product. After then, the qualities of selected crystals were briefly checked by a rapid scan, and the best crystal was chosen for the further data collection. Full data collection was processed using the Bruker APEX2 software [32]. Data reduction, integration, and unit-cell refinements were carried out using SAINT program [33], and semi-empirical absorption correction based on equivalents was conducted using the SADABS program [34]. The program XPREP in the SHELXTL software package was exploited to sort and merge the structure factors [35]. Refined parameters included the scale factor, atomic positions with anisotropic displacement parameters, extinction coefficients, and occupation factors of five Eu/Ca mixed-sites and one Ge/Sn mixed-site for $\text{Eu}_{3.04(4)}\text{Ca}_{5.96}\text{In}_8\text{Ge}_{7.77(2)}\text{Sn}_{0.23}$, and three Eu/Ca mixed-sites and one Ge/Sn mixed-site for $\text{Eu}_{0.95(1)}\text{Ca}_{2.05}\text{InGe}_{2.73(1)}\text{Sn}_{1.27}$ and $\text{Eu}_{1.02(1)}\text{Ca}_{1.98}\text{InGe}_{2.87(1)}\text{Sn}_{1.13}$, respectively.

During the structure refinement for two compounds in the $(\text{Eu}_{1-x}\text{Ca}_x)_3\text{In}(\text{Ge}_{3-y}\text{Sn}_{1+y})$ series, we found that the atomic displacement parameters (ADP) for the Sn1 sites were slightly higher than those of Ge and In sites. These Sn1 sites were crystallographically the identical sites to the In2 sites of the parental $(\text{Eu}/\text{Ca})_3\text{In}_2\text{Ge}_3$ phase [12], and the ADP for the In2 sites in the parental phase were also slightly higher than those of other In- and Ge-sites. Therefore, the larger ADP at the given site should be regarded as a structural characteristic of this type of structure. However, in order to clarify any possibility of a partial occupation or a Ge-mixed occupation for the Sn1-sites, we attempted to refine the crystal structures by allowing free occupations at the given site. However, as the occupations of the Sn1-sites were set free, the values became 99.7(2)% and 100.3(3)%, respectively, for $\text{Eu}_{1.02}\text{Ca}_{1.98}\text{InGe}_{2.87}\text{Sn}_{1.13}$ and $\text{Eu}_{0.95}\text{Ca}_{2.05}\text{InGe}_{2.73}\text{Sn}_{1.27}$, and the ADP were kept nearly constant. Thus, we concluded that there was no further reason to consider either a partial or a mixed-occupation for the Sn1 sites.

In the last refinement cycle, atomic positions were standardized using STRUCTURE TIDY [36]. Important crystallographic data, atomic positions, thermal displacement parameters, and selected interatomic distances are listed in Tables 1–3. CIF Files are deposited in Fachinfor-mationszentrum Karlsruhe, 76344 Eggenstein-Leopold-shafen, Germany (Fax: (49) 7247-808-666; E-mail: crysdata@fiz.karlsruhe.de) with depository numbers of CSD-429251 for $\text{Eu}_{3.04(4)}\text{Ca}_{5.96}\text{In}_8\text{Ge}_{7.77(2)}\text{Sn}_{0.23}$, CSD-429252 for $\text{Eu}_{1.02(1)}\text{Ca}_{1.98}\text{InGe}_{2.87(1)}\text{Sn}_{1.13}$ and CSD-429253 for $\text{Eu}_{0.95(1)}\text{Ca}_{2.05}\text{InGe}_{2.73(1)}\text{Sn}_{1.27}$.

Table 3. Selected interatomic distances (Å) for $\text{Eu}_{3.04(4)}\text{Ca}_{5.96}\text{In}_8\text{Ge}_{7.77(2)}\text{Sn}_{0.23}$, $\text{Eu}_{1.02(1)}\text{Ca}_{1.98}\text{InGe}_{2.87(1)}\text{Sn}_{1.13}$ and $\text{Eu}_{0.95(1)}\text{Ca}_{2.05}\text{InGe}_{2.73(1)}\text{Sn}_{1.27}$.

Atomic Pair	Distance		Atomic Pair	Distance	
	$\text{Eu}_{3.04(4)}\text{Ca}_{5.96}\text{In}_8\text{Ge}_{7.77(2)}\text{Sn}_{0.23}$			$\text{Eu}_{1.02(1)}\text{Ca}_{1.98}\text{InGe}_{2.87(1)}\text{Sn}_{1.13}$	$\text{Eu}_{0.95(1)}\text{Ca}_{2.05}\text{InGe}_{2.73(1)}\text{Sn}_{1.27}$
In1-Ge1/Sn(×2)	2.816(1)		In1-Ge2	2.779(1)	2.779(1)
In1-Ge1/Sn(×1)	2.896(2)		In1-Ge3/Sn2(×2)	2.811(1)	2.825(1)
In1-Ge2	2.770(1)		In1-Ge3/Sn2(×1)	2.898(1)	2.914(1)
In2-Ge1/Sn	3.270(1)		Sn1-Ge1	2.859(1)	2.861(1)
In2-Ge2	2.959(2)		Sn1-Ge1	2.947(1)	2.953(1)
In2-Ge3	2.981(2)		Sn1-Ge2	2.986(1)	2.987(1)
In2-Ge4	3.030(1)		Sn1-Ge3/Sn2	3.377(1)	3.377(1)
In3-Ge3	2.787(1)				
In3-Ge4	2.793(2)				
In3-In5	3.022(1)				
In4-Ge4	2.834(1)				
In4-In5	2.988(1)				
Ge2-Ge3	2.554(2)		Ge1-Ge2	2.536(1)	2.534(1)

3.3. Electronic Structure Calculations

Theoretical investigations have been carried out using two structural models with idealized compositions of “Eu₃Ca₆In₈Ge₇Sn” and “EuCa₂InGe₃Sn” representing for the (Eu_{1-x}Ca_x)₉In₈(Ge_{1-y}Sn_y)₈ and the (Eu_{1-x}Ca_x)₃In(Ge_{3-y}Sn_{1+y}) phases, respectively. The Stuttgart TB-LMTO47 program with the atomic sphere approximation (ASA) [25] was exploited, and exchange and correlation were treated by the local density approximation (LDA) [22]. All relativistic effects except spin-orbit coupling were taken into account by using a scalar relativistic approximation. In the ASA method, space is filled with overlapping Wigner-Seitz (WS) atomic spheres [25], and the symmetry of the potential is considered spherical inside each WS sphere. A combined correction is used to take into account the overlapping part [37]. The radii of WS spheres were determined by an automatic procedure and by requiring the overlapping potential be the best possible approximation to the full potential [37]. This overlap should not be too large because the error in kinetic energy introduced by the combined correction is proportional to the fourth power of the relative sphere overlap. No empty sphere [25] was necessary. The used WS radii for each model are listed as follows: Eu = 1.94–2.17 Å, Ca = 1.99–2.11 Å, In = 1.60–1.92 Å, Ge = 1.48–1.61 Å, and Sn = 1.66 Å for Eu₃Ca₆In₈Ge₇Sn; and Eu = 2.18 Å, Ca = 2.02–2.08 Å, In = 1.62 Å, Ge = 1.45–1.58 Å, and Sn = 1.81 Å for EuCa₂InGe₃Sn. The basis sets included 6s, 6p and 5d orbitals for Eu; 4s, 4p and 3d orbitals for Ca; 5s, 5p and 5d orbitals for In; 4s, 4p and 4d orbitals for Ge; and 5s, 5p and 5d orbitals for Sn for both models. The Eu 5d, Ca 3d, In 5d, and Ge 4d orbitals were treated by the Löwdin downfolding technique [25]. The 4f wave functions of Eu were treated as core functions. The *k*-space integrations were conducted by the tetrahedron method [38], and the self-consistent charge density was obtained using 360 and 216 irreducible *k*-points in the Brillouin zone, respectively, for Eu₃Ca₆In₈Ge₇Sn and EuCa₂InGe₃Sn.

3.4. EDS and SEM Images Analyses

Elemental analysis via EDS and product images of single-crystals were taken by ULTRA Plus field-emission SEM system (Zeiss, Oberkochen, Germany) with an acceleration voltage of 30 kV. Several bar-/needle-shaped single-crystals were selected from each product batch, and those crystals were carefully mounted on the circumference of an aluminum puck with double-sided conducting carbon tapes inside an argon-filled glove-box. EDS results are as follows: Eu_{3.27(9)}Ca_{5.68}In_{8.49}Ge_{7.80}Sn_{0.24}, Eu_{1.18(9)}Ca_{1.84}In_{1.45}Ge_{2.75}Sn_{0.80}, and Eu_{0.98(9)}Ca_{2.03}In_{1.54}Ge_{2.53}Sn_{0.92}, and these values are comparable to the refined SXRD results as follows: Eu_{3.04(4)}Ca_{5.96}In₈Ge_{7.77(2)}Sn_{0.23}, Eu_{1.02(1)}Ca_{1.98}InGe_{2.87(1)}Sn_{1.13}, and Eu_{0.95(1)}Ca_{2.05}InGe_{2.73(1)}Sn_{1.27}. Some deviations of In contents in both title phases can be attributed to the remaining In-flux metals stuck on samples.

3.5. DSC Measurement

Thermal characteristic of Eu_{1.02(1)}Ca_{1.98}InGe_{2.87(1)}Sn_{1.13} was investigated by DSC using the TA instruments DSC2910 (TA Instruments, New Castle, DE, USA). The sample was enclosed in an aluminum container and heated from 300 up to 773 K at 10 K/min, then cooled down to 300 K at 10 K/min under N₂ atmosphere.

3.6. Magnetic Property Measurements

Magnetization of $\text{Eu}_{1.02(1)}\text{Ca}_{1.98}\text{InGe}_{2.87(1)}\text{Sn}_{1.13}$ was measured by MPMS-7 using a polycrystalline sample weighing *ca.* 60 mg. To investigate the dc magnetization, the measurement was initially performed on heating the sample from 25 to 300 K under zero-field-cooled condition (ZFC). The measurement was repeated upon cooling from 300 to 5 K with a magnetic field of 10 kOe under field-cooled condition (FC).

4. Conclusions

Three Sn-substituted quinary polar intermetallic compounds in the $(\text{Eu}_{1-x}\text{Ca}_x)_9\text{In}_8(\text{Ge}_{1-y}\text{Sn}_y)_8$ and the $(\text{Eu}_{1-x}\text{Ca}_x)_3\text{In}(\text{Ge}_{3-y}\text{Sn}_{1+y})$ series have been synthesized using the molten In-metal flux method and characterized by both powder and single-crystal X-ray diffractions. $\text{Eu}_{3.04(4)}\text{Ca}_{5.96}\text{In}_8\text{Ge}_{7.77(2)}\text{Sn}_{0.23}$ adopted its parental $\text{Eu}_{2.94(2)}\text{Ca}_{6.06}\text{In}_8\text{Ge}_8$ -type structure, and the overall crystal structure was viewed as an assembly of the 3D polyanionic framework consisting of the 1D $\text{In}(\text{Ge}/\text{Sn})_4$ tetrahedral chain, the annulene-like 12-membered rings and the bridging Ge_2 dimers, and the space filling mixed-Eu/Ca cations. The 12-membered ring can alternately be viewed as a combination of two different types of 1D anionic chain, the *zig-zag* and the *cis-trans*, propagating orthogonal directions to each other. Since the partial Sn-substitution for Ge was confined at the Ge1 site in the $\text{In}(\text{Ge}/\text{Sn})_4$ tetrahedron, the overall size of a unit cell as well as various interatomic distances were not much enlarged. Five mixed-cationic sites were locally surrounded by either 9 or 10 anions, respectively, forming a distorted pyramid or pentagonal-prisms. On the other hand, two derivatives in the $(\text{Eu}_{1-x}\text{Ca}_x)_3\text{In}(\text{Ge}_{3-y}\text{Sn}_{1+y})$ phase were obtained as the loaded Sn content increased up to equal to or slightly higher than that of Ge. Unlike the parental phase, two derivatives were successfully crystallized in the given structure type even when the loaded Eu:Ca ratio was nearly 1:2. In addition, the overall atomic % of Eu included in compounds also increased up to 34 atomic %, which exceeded the previously claimed maximum limit of 20 atomic %. The rationale for this phenomenon should be attributed to the atomic size-factor: the Sn-substitution for Ge both in the $\text{In}(\text{Ge}/\text{Sn})_4$ tetrahedron and the 1D *cis-trans* chain caused polyanionic frameworks to expand resulting in accommodating extra amounts of larger-size Eu in compounds.

A series of theoretical investigations was conducted using two structural models of $\text{Eu}_3\text{Ca}_6\text{In}_8\text{Ge}_7\text{Sn}$ and $\text{EuCa}_2\text{InGe}_3\text{Sn}$. The resultant DOS and COHP analyses indicated overall significant valence orbital mixings of all five components throughout the entire energy window and implied semi-metallic characters for both title phases. The temperature-dependent magnetization measurement for $\text{Eu}_{1.02(1)}\text{Ca}_{1.98}\text{InGe}_{2.87(1)}\text{Sn}_{1.13}$ proved the effective magnetic moment of $7.34 \mu_B$ per Eu^{2+} ion and a low temperature FM ordering of Eu with $\theta_P = +3.32$ K. The relatively low value of an effective magnetic moment was attributed to the presence of remaining In metals in a product. The DSC measurement also confirmed that there existed no secondary phase in $\text{Eu}_{1.02(1)}\text{Ca}_{1.98}\text{InGe}_{2.87(1)}\text{Sn}_{1.13}$ and no structural transformation or decomposition within the measured temperature range.

Acknowledgments

This work was supported by the research grant of Chungbuk National University in 2012.

Author Contributions

Hyein Woo and Eunyoung Jang conducted synthesis and characterization of title compounds as well as theoretical studies. Jin Kim and Yunho Lee collected single-crystal X-ray diffraction data. Jongsik Kim analyzed the magnetization data. Tae-Soo You supervised the overall research process. Tae-Soo You and Hyein Woo wrote a manuscript. All authors read and proved the manuscript.

Conflicts of Interest

The authors declare no conflict of interest.

References

1. Kanatzidis, M.G. *Recent Trends in Thermoelectric Materials Research I*, Series: Semiconductors and Semimetals; Academic: San Diego, CA, USA, 2001; Volume 69, p. 51.
2. Condrón, C.L.; Kauzlarich, S.M.; Nolas, G.S. Structure and thermoelectric characterization of $A_x\text{Ba}_{8-x}\text{Al}_{14}\text{Si}_{31}$ ($A = \text{Sr}, \text{Eu}$) Single crystals. *Inorg. Chem.* **2007**, *46*, 2556–2562.
3. Snyder, G.J.; Toberer, E.S. Complex thermoelectric materials. *Nat. Mater.* **2008**, *7*, 105–114.
4. Gschneidner, K.A., Jr.; Pecharsky, V.K.; Tsokol, A.O. Recent developments in magnetocaloric materials. *Rep. Prog. Phys.* **2005**, *68*, 1479–1539.
5. Morrelon, L.; Blasco, J.; Algarabel, P.A.; Ibarra, M.R. Nature of the first-order antiferromagnetic-ferromagnetic transition in the Ge-rich magnetocaloric compounds $\text{Gd}_5(\text{Si}_x\text{Ge}_{1-x})_4$. *Phys. Rev. B* **2000**, *62*, 1022–1026.
6. Morellon, L.; Stankiewicz, J.; Garcia-Landa, B.; Algarabel, P.; Ibarra, M.R. Giant magnetoresistance near the magnetostructural transition in $\text{Gd}_5(\text{Si}_{1.8}\text{Ge}_{2.2})$. *Appl. Phys. Lett.* **1998**, *73*, 3462.
7. Sarkar, S.; Peter, S. Structural phase transitions in a new compound Eu_2AgGe_3 . *Inorg. Chem.* **2013**, *52*, 9741–9748.
8. Aynajian, P.; da Silva Neto, E.H.; Gyenis, A.; Baumbach, R.E.; Thompson, J.D.; Fisk, Z.; Bauer, E.D.; Yazdani, A. Visualizing heavy fermions emerging in a quantum critical Kondo lattice. *Nature* **2012**, *486*, 201–206.
9. Custers, J.; Lorenzer, K.-A.; Müller, M.; Prokofiev, A.; Sidorenko, A.; Winkler, H.; Strydom, A.M.; Shimura, Y.; Sakakibara, T.; Yu, R.; *et al.* Destruction of the Kondo effect in the cubic heavy-fermion compound $\text{Ce}_3\text{Pd}_{20}\text{Si}_6$. *Nat. Mater.* **2012**, *11*, 189–194.
10. Tran, V.H.; Kaczorowski, D.; Khan, R.T.; Bauer, E. Superconductivity and non-Fermi-liquid behavior of Ce_2PdIn_8 . *Phys. Rev. B* **2011**, *83*, 064504.
11. Shim, J.H.; Haule, K.; Kotliar, G. Modeling the localized-to-itinerant electronic transition in the heavy fermion system CeIrIn_5 . *Science* **2007**, *318*, 1615–1617.
12. You, T.-S.; Tobash, P.H.; Bobev, S. Mixed cations and structural complexity in $(\text{Eu}_{1-x}\text{Ca}_x)_4\text{In}_3\text{Ge}_4$ and $(\text{Eu}_{1-x}\text{Ca}_x)_3\text{In}_2\text{Ge}_3$ —The first two members of the homologous series $A_{2[n+m]}\text{In}_{2n+m}\text{Ge}_{2[n+m]}$ ($n, m = 1, 2, \dots, \infty$; $A = \text{Ca}, \text{Sr}, \text{Ba}, \text{Eu}, \text{or Yb}$). *Inorg. Chem.* **2010**, *49*, 1773–1783.
13. Sumanta, S.; Matthias, J.G.; Sebastian, C.P. Crystal structure and magnetic properties of indium flux grown EuAu_2In_4 and EuAuIn_4 . *Cryst. Growth Des.* **2013**, *13*, 4285–4294.

14. Woo, H.; Nam, G.; Jang, E.; Kim, J.; Lee, Y.; Ahn, K.; You, T.-S. Single-crystal growth and size control of three novel polar intermetallics: $\text{Eu}_{2.94(2)}\text{Ca}_{6.06}\text{In}_8\text{Ge}_8$, $\text{Eu}_{3.13(2)}\text{Ca}_{5.87}\text{In}_8\text{Ge}_8$, and $\text{Sr}_{3.23(3)}\text{Ca}_{5.77}\text{In}_8\text{Ge}_8$ with crystal structure, chemical bonding, and magnetism studies. *Inorg. Chem.* **2014**, *53*, 4669–4677.
15. Jeon, B.; Jeon, J.; Lee, J.; Kim, J.; You, T.-S. Experimental and theoretical investigations for site-preference and anisotropic size-change of $\text{RE}_{11}\text{Ge}_4\text{In}_{6-x}\text{M}_x$ ($\text{RE} = \text{La, Ce}$; $\text{M} = \text{Li, Ge}$; $x = 1, 1.96$). *J. Alloys Compd.* **2015**, *620*, 269–276.
16. Nam, G.; Jang, E.; You, T.-S. Site-preference among three anions in the quaternary BaAl_4 -type structure: Experimental and computational investigations for $\text{BaLi}_{1.09(1)}\text{In}_{0.91}\text{Ge}_2$. *Bull. Korean Chem. Soc.* **2013**, *34*, 3847–3850.
17. Nam, G.; Jeon, J.; Kim, Y.; Kang, S.; Ahn, K.; You, T.-S. Combined effect of chemical pressure and valence electron concentration through the electron-deficient Li-substitution on the RE_4LiGe_4 ($\text{RE} = \text{La, Ce, Pr and Sm}$) system. *J. Solid State Chem.* **2013**, *205*, 10–20.
18. You, T.-S.; Jung, Y.; Han, M.-K.; Miller, G. The $\text{Y}_{5-x}\text{Mg}_{24+x}$ ($1.08(4) < x < 1.30(1)$) series and a ternary derivative $\text{Ce}_{6.9}\text{Y}_{12.5(7)}\text{Mg}_{92.2}$: A comparison of their crystal and electronic structures. *J. Solid State Chem.* **2013**, *204*, 170–177.
19. Jung, Y.; Nam, G.; Jeon, J.; Kim, Y.; You, T.-S. Crystal structure and chemical bonding of novel Li-containing polar intermetallic compound $\text{La}_{11}\text{Li}_{12}\text{Ge}_{16}$. *J. Solid State Chem.* **2012**, *196*, 543–549.
20. You, T.-S.; Bobev, S. Synthesis and structural characterization of $\text{A}_3\text{In}_2\text{Ge}_4$ and $\text{A}_5\text{In}_3\text{Ge}_6$ ($\text{A} = \text{Ca, Sr, Eu, Yb}$)—New intermetallic compounds with complex structures, exhibiting Ge–Ge and In–In bonding. *J. Solid State Chem.* **2010**, *183*, 1258–1265.
21. Andersen, O.K. Linear methods in band theory. *Phys. Rev. B* **1975**, *12*, 3060–3083.
22. Andersen, O.K.; Jepsen, O. Explicit, First-principles tight-binding theory. *Phys. Rev. Lett.* **1984**, *53*, 2571–2574.
23. Lambrecht, W.R.L.; Andersen, O.K. Minimal basis sets in the linear muffin-tin orbital method: Application to the diamond structure crystals carbon, silicon, and germanium. *Phys. Rev. B* **1986**, *34*, 2439–2449.
24. Jepsen, O.; Burkhardt, A.; Andersen, O.K. *The TB-LMTO-ASA Program*, version 4.7; Max-Planck-Institut für Festkörperforschung: Stuttgart, Germany, 1999.
25. Andersen, O.K.; Jepsen, O.; Glötzel, D. In *Highlights of Condensed Matter Theory*; Bassani, F., Fumi, F., Tosi, M., Eds.; North-Holland, Lambrecht; Worland, WY, USA, 1985.
26. Dronskowski, R.; Blöchl, P. Crystal orbital Hamilton populations (COHP): Energy-resolved visualization of chemical bonding in solids based on density-functional calculations. *J. Phys. Chem.* **1993**, *97*, 8617–8624.
27. Emsley, J. *The Elements*; Clarendon Press: Oxford, UK, 1990.
28. Putz, M.V. Markovian approach of the electron localization functions. *Int. J. Quant. Chem.* **2005**, *105*, 1–11.
29. Putz, M.V. Density functionals of chemical bonding. *Int. J. Mol. Sci.* **2008**, *9*, 1050–1095.
30. Putz, M.V. Path integrals for electronic densities, reactivity indices, and localization functions in quantum systems. *Int. J. Mol. Sci.* **2009**, *10*, 4816–4940.

31. Hunter B.A. *International Union of Crystallography, Commission for Powder Diffraction*, Newsletter 20; IUCr: Chester, UK, 1998; p. 21.
32. *APEX2*; Bruker Analytical X-ray Systems, Inc.: Madison, WI, USA, 2007.
33. *SAINT*; Bruker Analytical X-ray Systems, Inc.: Madison, WI, USA, 2002.
34. Sheldrick, G.M. *SADABS*; University of Göttingen: Göttingen, Germany, 2003.
35. Sheldrick, G.M. *SHELXTL*; University of Göttingen: Göttingen, Germany, 2001.
36. Gelato, L.M.; Parthe, E. STRUCTURE TIDY—A computer program to standardize crystal structure data. *J. Appl. Crystallogr.* **1987**, *20*, 139–143.
37. Jepsen, O.; Andersen, O.K. Calculated electronic structure of the sandwich^d metals LaI₂ and CeI₂: Application of new LMTO techniques. *Z. Phys. B* **1995**, *97*, 35–47.
38. Blöchl, P.E.; Jepsen, O.; Andersen, O.K. Improved tetrahedron method for Brillouin-zone integrations. *Phys. Rev. B* **1994**, *49*, 16223–16233.

© 2015 by the authors; licensee MDPI, Basel, Switzerland. This article is an open access article distributed under the terms and conditions of the Creative Commons Attribution license (<http://creativecommons.org/licenses/by/4.0/>).